9-2004

Mushy-Zone Rayleigh Number to Describe Macrosegregation and Channel Segregate Formation During Directional Solidification of Metallic Alloys

Surendra N. Tewari
Cleveland State University, s.tewari@csuohio.edu

R. Tiwari
Cleveland State University

G. Magadi
American Bureau of Shipping

Publisher's Statement

Original Citation

Tewari, S.N., Tiwari, R., & Magadi, G. (2004). Mushy-Zone Rayleigh Number to Describe Macrosegregation and Channel Segregate Formation During Directional Solidification of Metallic Alloys. Metallurgical and Materials Transactions A: Physical Metallurgy and Materials Science **35A**, 2927-2934.

Repository Citation

Mushy-Zone Rayleigh Number to Describe Macrosegregation and Channel Segregate Formation during Directional Solidification of Metallic Alloys

S.N. TEWARI, R. TIWARI, and G. MAGADI

A recently defined mushy-zone Rayleigh number (R_{aM}) that includes side-branching contributions to the mushy-zone permeability has been examined for its correlation with the longitudinal macrosegregation and channel segregate formation. The Rayleigh number shows (1) a strong correlation between the extent of longitudinal macrosegregation and increase in the mushy-zone convection and (2) a good ability to predict the formation of channel segregates during directional solidification.

I. INTRODUCTION

DIRECTIONAL solidification of alloys, such as hypoeutectic Pb-Sn or Pb-Pb, where solute enrichment causes a reduced melt density, in a positive thermal gradient, with melt on top and solid below, produces a density inversion in the melt, both in the mushy zone and in the overlying liquid immediately ahead of the dendritic array tips. This causes convection that produces macrosegregation along the sample length;[1,2] when severe, it also produces channel segregates (or freckles).[3–13] Based on the measurements of dendrite specific surface area (S_v) in the quenched mushy zone of directionally solidified Pb-Sb and Pb-Sn alloys, we recently reported[14] that $S_v = \lambda_1^{-1} S^{*-0.33} (3.38 - 3.29\phi + 8.85\phi^2)$, where λ_1 is primary dendrite spacing, ϕ is fraction interdendritic liquid, and $S^* = D_l G_{eff}/[V m_l C_o (k-1)/k]$, with D_l being solutal diffusivity in the melt, G_{eff}, the effective thermal gradient, V, the growth speed, m_l, the liquidus slope, C_o, the solute content of the melt, and k the solute partition coefficient. Incorporation of the above S_v dependence into the Kozney–Carman permeability (κ) of a porous bed, $\kappa = \phi^3/4.2\, S_v^2 (1-\phi)^2$,[15] yielded a relationship that describes the processing parameter dependence of mushy-zone permeability during directional solidification. Using this permeability, a mushy-zone Rayleigh number, R_{aM}, was defined following the procedure described by Beckermann *et al.*[16] Since convection is known to be localized in the immediate vicinity of dendrite tips,[17] it was assumed[14] that the Rayleigh number calculated in the mush at a distance equal to 30 times the dendrite tip radius can be used to represent convection in the mushy zone. The tip radius and spacing of primary dendrites used in these calculations were those predicted by the model attributed to Hunt–Lu.[18] In a recent publication,[14] it was demonstrated that R_{aM}, which includes side-branching contribution to the mushy-zone permeability, shows a marked improvement in correlating the extent of primary spacing decrease with increasing convection as compared with R_{aB}, the Rayleigh number used by Beckerman *et al.*,[16] which used a different permeability relationship.

An appropriately defined mushy-zone Rayleigh number must be able to describe three important experimental observations. It should be able to correlate the extent of natural convection with the experimentally observed reduction in primary dendrite spacing;[19–21] it should be able to relate the intensity of mushy-zone convection during directional solidification and the resulting longitudinal macrosegregation;[1,2] and it should be useful in predicting the onset of channel segregate formation.[3–13] The purpose of this article is to demonstrate that R_{aM} describes the extent of longitudinal macrosegregation and predicts the onset of channel segregate formation better as compared with R_{aB}, even though the only difference between the two is the use of a different mushy-zone permeability relationship.

II. EXPERIMENTAL

A range of alloy compositions (Pb-2.2 and 5.8 wt pct Sb, Pb-10 to 54.7 wt pct Sn) were directionally solidified (DS) in a flowing argon atmosphere at several thermal gradients (ranging from 10 to 197 K cm^{-1}) and growth speeds (ranging from 2 to 157 μm s^{-1}) in 0.7-cm i.d. quartz ampoules in a furnace arrangement where the furnace was translated and the sample was kept stationary.[13] Some samples were also DS in 1.8-cm i.d. quartz ampoules to examine the influence of crucible diameter on the formation of channel segregates and the associated longitudinal macrosegregation. Most of the samples were quenched after 9 to 10 cm of directional solidification; melt column length at the onset of directional solidification was 18 to 20 cm. Macrosegregation was measured by chemical analysis of thin slices that were cut along the directionally solidified length of the sample and from its quenched liquid portion. Transverse microstructures were examined to characterize the surface and internal channel segregates and their distribution along the directionally solidified length. Several growth speed change, step increase and step decrease in the speed, experiments were also carried out to precisely identify the solidification conditions necessary for the formation of channel segregates.

III. RESULTS

A. *Typical Microstructures*

Figure 1 shows typical transverse microstructures observed in Pb-5.8 wt pct Sb alloys DS at 40 K cm^{-1}. At a low growth

S.N. TEWARI, Professor, and R. TIWARI, Graduate Student, are with the Chemical and Biomedical Engineering Department, Cleveland State University, Cleveland, OH 44115. Contact e-mail: s.tewari@csuohio.edu G. MAGADI, formerly Research Associate, Chemical Engineering Department, Cleveland State University, is Senior Engineer, American Bureau of Shipping, Houston, TX 77060.

Manuscript submitted June 16, 2003.

speed of 3 μm s^{-1} (Figure 1(a)), there is an interior channel segregate present in the sample. An interior channel segregate was also observed at 5 μm s^{-1}. At a higher growth speed of 10 μm s^{-1} (Figure 1(b)), there is no channel segregate, but there is significant nonuniformity in the interdendritic volume fraction liquid; the region marked by the arrow has more liquid fraction as compared with the remainder of the sample cross section. This nonuniformity is not present at higher growth speeds; for example, at 30 μm s^{-1} (Figure 1(c)), dendrites are uniformly distributed throughout the entire sample cross section.

Experiments showed that at 3 μm s^{-1}, several segregates appear within a solidification distance of 1 cm; the mushy-zone length for this growth condition is about 0.9 cm. The number of channel segregates and their location on the sample cross section, however, change along the DS length; channels meander on the sample cross section, existing ones merge, and new ones form during directional solidification. Examination of samples with growth speed step change showed that internal and surface channels that formed at 3 μm s^{-1} vanished within about 1 cm distance after the speed was increased to 10 μm s^{-1}. Similarly, samples growing at 30 μm s^{-1} did not have channel segregates, but channels formed within about 1 cm after the speed was decreased to 3 μm s^{-1}. Serial sectioning through quenched mushy zone demonstrated that internal channel segregates invariably extend from the tips of the dendrite array to its very base.

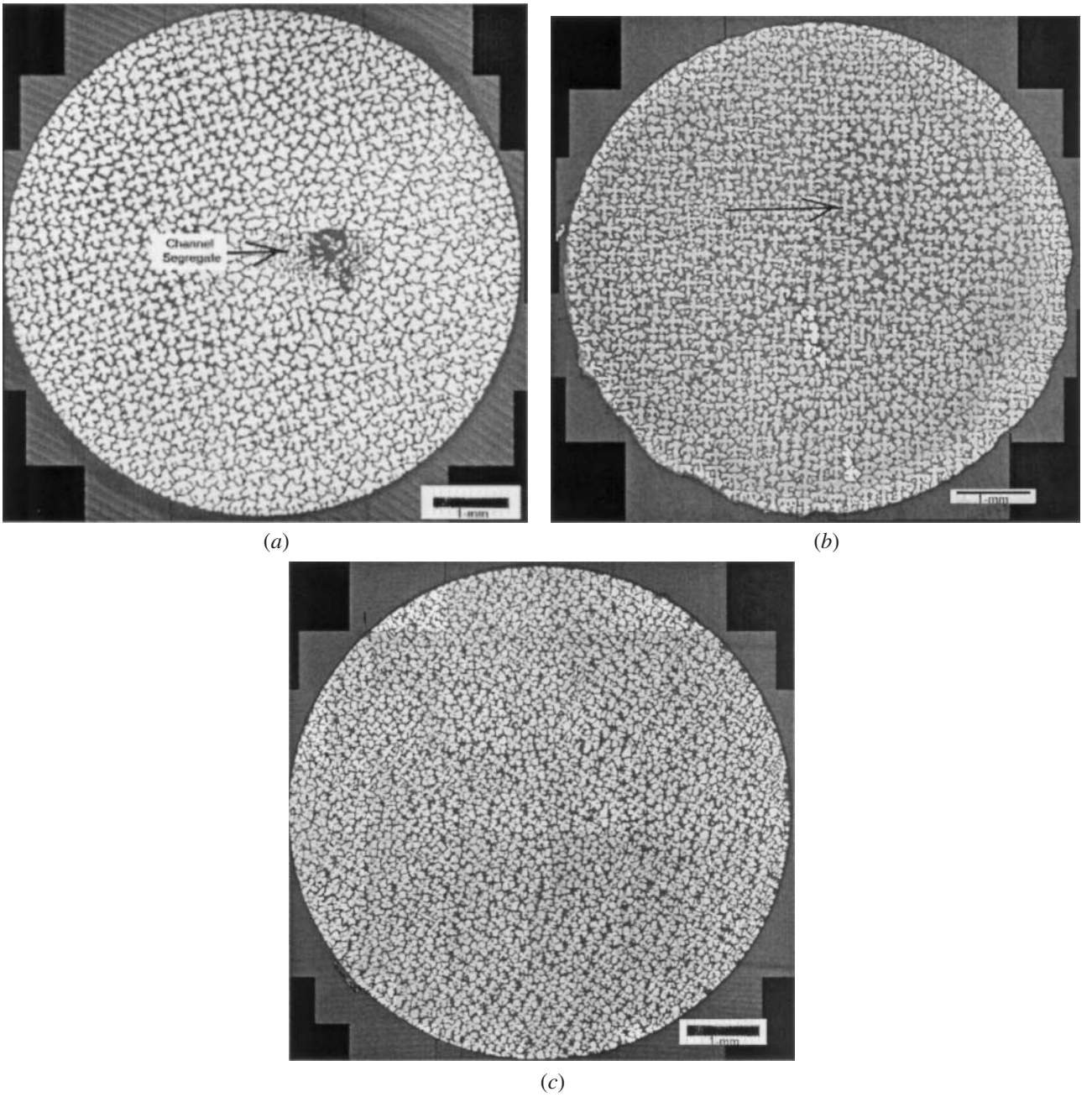

(*a*) (*b*) (*c*)

Fig. 1—Transverse microstructure of Pb-5.8 wt pct Sb alloy samples directionally solidified at 40 K cm^{-1}. (*a*) Interior channel segregates at a growth speed of 3 μm s^{-1}. (*b*) Absence of segregates at 10 μm s^{-1}; presence of large inhomogeneity in the interdendritic liquid fraction shows a tendency for channel formation. (*c*) No channel segregates at 30 μm s^{-1}.

B. *Influence of Crucible Diameter*

Figure 2(a) shows the microstructure of a Pb-33.4 wt pct Sn alloy sample grown in a 0.7-cm i.d. quartz crucible at 75 K cm^{-1} with a growth speed of 8 μm s^{-1}. It does not have internal channel segregate; instead, it has two segregates located on the sample surface, marked by arrows. In order to examine if an increase in sample diameter would push the segregates from the sample surface into its interior, a similar alloy (Pb-32 wt pct Sn) was grown in a 1.8-cm i.d. quartz crucible under similar growth conditions (60 K cm^{-1}, 8 μm s^{-1}). The 0.7- and 1.8-cm i.d. samples had similar primary dendrite spacing, 166 and 159 μm, respectively. Figure 2(b) shows that the larger diameter sample also did not have internal channel segregates. However, it has significantly more surface segregates (marked by arrows), nine versus two for the small diameter sample. This indicates a more intense convective mixing between the mushy zone and the overlying liquid during directional solidification of the 1.8-cm i.d. sample than the 0.7-cm one. This is also confirmed by the longitudinal macrosegregation observed in the two samples (Figure 3(a)). Figure 3(a) plots the ratio of the tin content along the DS length (C_s) and C_o, the initial solute content of the melt, as a function of fraction

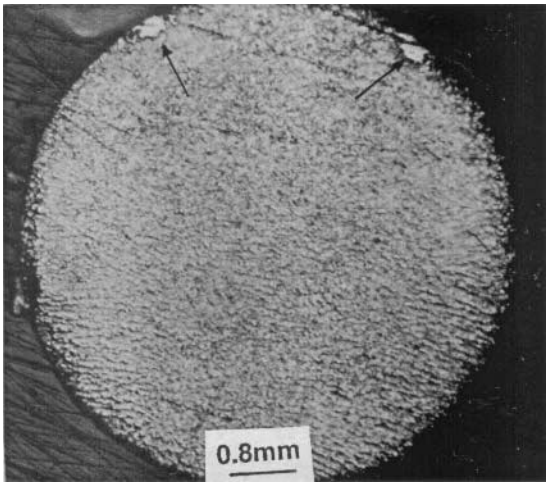

(*a*)

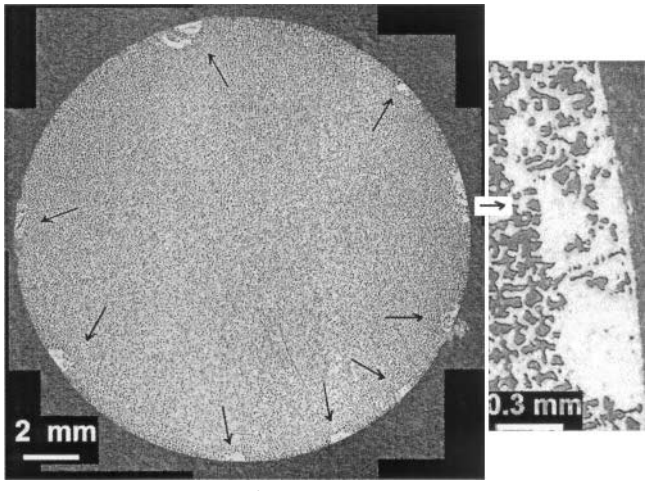

(*b*)

Fig. 2—Influence of crucible diameter on the surface channel segregate formation in a directionally solidified Pb-Sn alloy. (*a*) Pb-33.4 wt pct Sn, 0.7-mm-diameter sample, 75 K cm^{-1} and 8 μm s^{-1}, shows one surface channel segregate. (*b*) Pb-32 wt pct Sn, 1.8-cm-diameter sample, 60 K cm^{-1} and 8 μm s^{-1}, shows nine surface channel segregates.

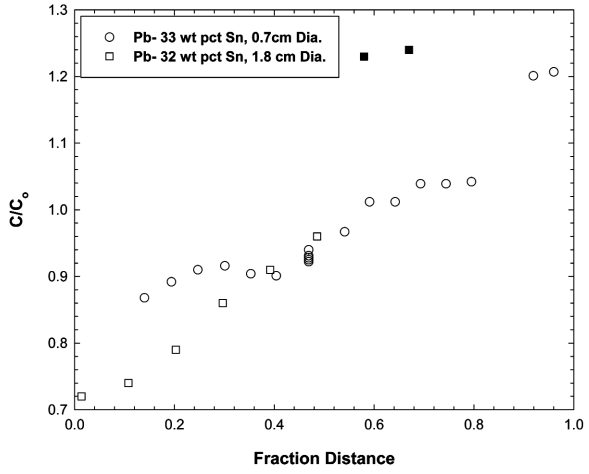

(*a*)

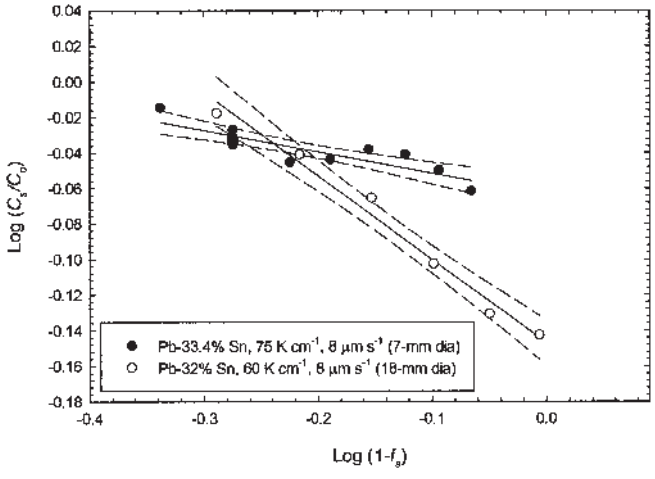

(*b*)

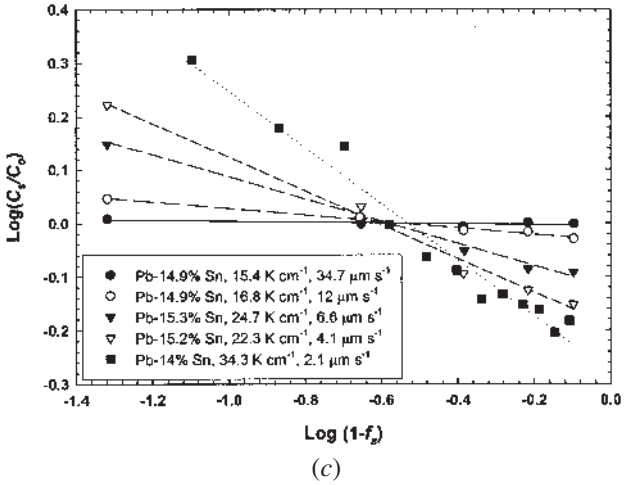

(*c*)

Fig. 3—Macrosegregation along the DS length for the small and large diameter samples containing surface freckles. (*a*) Composition as a function of distance. (*b*) Log (C_s/C_o) *vs* log ($1 - f_s$). (*c*) Log (C_s/C_o) *vs* log ($1 - f_s$) for the macrosegregation data from the end-quench directional solidification experiments of Wang *et al.*[8,9]

distance solidified. Open symbols correspond to the DS portion of the sample and filled symbols to the liquid portion, which was quenched at the end of directional solidification. The 1.8-cm i.d. sample, indicated by square symbols, was quenched after solidifying about 50 pct of its initial melt column length, whereas the 0.7-cm i.d. sample, indicated by circles, was quenched after solidifying about 80 pct. In the absence of convective mixing, C_s/C_o would be expected to be unity along the entire sample length. It is apparent that the larger diameter sample has more macrosegregation.

As reported earlier,[1,2] the effective partition coefficient, k_e, obtained by fitting experimentally observed macrosegregation to $C_s/C_o = k_e\,(1 - f_s)^{(k_e - 1)}$ is a good indicator of the extent of convective mixing during directional solidification. Figure 3(b) plots log (C_s/C_o) *vs* log $(1 - f_s)$ for the data shown in Figure 3(a). It also includes linear least-squares fit through the data, indicated by solid lines, and the corresponding 95 pct confidence intervals (broken lines). Macrosegregation data show a good fit to $C_s/C_o = k_e\,(1 - f_s)^{(k_e - 1)}$ relationship. Average k_e values (average of k_e obtained from the slope and that from the intercept) for the small and large diameter samples are 0.87 and 0.62, respectively.

IV. DISCUSSION

Table I lists the identification number of the samples, C_o, G_l, V, λ_{Expt} (experimentally measured primary dendrite spacing), G_{eff}, S^*, and R_t (dendrite tip radius) and λ_{Theory} (primary dendrite spacing) predicted from the Hunt–Lu model[18]) for those Pb-Sb and Pb-Sn alloy samples where macrosegregation data were available. The table also lists corresponding k_e, R_{aB}, and R_{aM} values. The next column in the table denotes the nature of channel segregates, surface or interior, and their number. Absence of data in this column indicates a channel-free microstructure. The table also includes data extracted from the literature on Pb-Sn,[1,2,5–9,12] Pb-Sb,[2,7] and Al-Mg[11] alloys; the last column provides the corresponding references. Please note that tip composition (C_t), tip radius, and primary spacing (λ_1) values used in calculating R_{aB} and R_{aM} in this table are those predicted from the Hunt–Lu model.[18] Our Pb-Sb alloy data (0.7-cm diameter 20-cm long cylindrical samples), data from Streat and Weinburg[5] (1.3-cm diameter, 14-cm long), data from Mori and Keisaku[11] (2.6-cm diameter, 20-cm long), and those from Grugel *et al*.[12] (0.5-cm diameter, 20-cm long) are from steady-state directional solidification experiments where either the cylindrical sample or the furnace setup was translated at a constant speed while the thermal gradient remained constant. The sample length for these experiments is usually several times larger than the mushy-zone length, whereas data from Sarazin and Hellawell[6] and Sarazin[7] (3.8-cm-diameter, 12-cm-long samples), from Wang and co-workers[8,9] (2-cm diameter, 5-cm long), and from Bergman *et al*.[10] (3.5-cm diameter, 6.3-cm long) are from end-quench type directional solidification experiments where melt was poured into a ceramic mold, heated from the top and cooled from bottom, and directional solidification was achieved by slow controlled cooling of the furnace. The sample length for these experiments was usually smaller than the mushy-zone length expected from their corresponding reported thermal gradient and growth speed values. Since thermal gradients and growth speeds did not remain constant during solidification of these samples, we have used their reported average values. Also, since thermal gradients for these experiments were measured within the mushy zone itself, their G_{eff} have been assumed to be the same as the corresponding reported thermal gradients.

Strictly speaking, the Rayleigh number definition presented above is valid only for steady-state directional solidification experiments; however, we will use R_{aB} and R_{aM} to examine data from end-quench DS experiments also.

A. *Macrosegregation*

As typically shown in Figure 3(c) for the data reported by Wang and co-workers[8,9] the $C_s/C_o = k_e\,(1 - f_s)^{(k_e - 1)}$ relationship described earlier for steady-state directional solidification experiments is also applicable for the end-quench DS experiments where ingots are less than one mushy zone long. Here, the reported macrosegregation data are replotted as log (C_s/C_o) *vs* log $(1 - f_s)$. Table I includes k_e values obtained from similar plots for end-quench DS experiments of Wang *et al*.[8,9] and Sarazin and Hellawell[6] and Sarazin.[7]

Figure 4(a) plots k_e as a function of R_{aB} for DS hypoeutectic Pb-Sn and Pb-Sb alloys. It contains data from 38 different directional solidification experiments, including data from our experiments (SNT), those from Wang *et al*.,[8] and those from Sarazin *et al*.[6,7] It also includes data from Mason *et al*. (MVT).[22] However, for MVT, the k_e values are not obtained from log (C_s/C_o) *vs* log $(1 - f_s)$ plots; instead, the ratio of the reported solid and liquid compositions at the quenched liquid-solid interface has been assumed to be equal to k_e. Even though the k_e *vs* R_{aB} plot shows the expected association between increasing macrosegregation (smaller k_e) and increasing convection (larger R_{aB}), there is a large scatter present. A much stronger association and decreased scatter becomes evident, however, when the same data are plotted as a function of R_{aM} (Figure 4(b)). This is demonstrated by a larger Spearman rank correlation coefficient for Figure 4(b), -0.71 with a p value of 0.000, as compared with -0.51 with a p value of 0.0012 in Figure 4(a).

B. *Formation of Channel Segregate*

Figure 5 compiles channel segregate formation data presented in Table I from several investigators and plots the corresponding Rayleigh numbers, R_{aB} in Figure 5(a) and R_{aM} in Figure 5(b). Open circles correspond to samples without channel segregates, filled circles indicate internal channel segregates, and filled squares indicate surface channels. This figure includes data from our research on Pb-Sb and Pb-Sn alloys DS in 0.7-cm i.d. crucibles, marked as SNT in Figure 5. The SNT sets also contain many samples that are not listed in Table I, especially no channel segregate samples, which were already included in a recent publication.[14] Data marked as Song-SNT are for Pb-32 and Pb-41.9 wt pct Sn alloy samples that were DS in 1.8-cm i.d. crucibles. This figure includes data from 102 separate directional solidification experiments in Pb-Sb, Pb-Sn, and Al-Mg alloys including 74 steady state and 28 end-quench DS type of experiments.

Figure 5(a) shows that R_{aB} does not yield a demarcation between channel segregate formation and its absence; this

Table I. Growth Parameters and Rayleigh Numbers for Directionally Solidified Pb-Sb, Pb-Sn, and Al-Mg Alloys*

Sample	C_o (Wt Pct)	G_l (K cm^{-1})	V (μm s^{-1})	λ_{Expt} (μm)	G_{eff} (K cm^{-1})	S*	R_t (μm)	λ_{Theory} (μm)	k_e	R_{aB}	R_{aM}	Freckle	Reference
Ding (6Sb9)	Pb-5.8Sb	140	3	163	95.6	0.1098	11.5	527.4	0.81	0.08453	0.1868	—	—
Ding (6Sb3)	Pb-5.8Sb	140	10	170	95.6	0.033	5.9	348.6	0.906	0.0377	0.02619	—	—
Kunal	Pb-5.8Sb	82	2.5	202	56	0.0772	12.3	696.0	—	0.2552	0.37149	Surf-1	—
Hui	Pb-5.8Sb	40	3	227.1	27.3	0.0314	11.0	873.1	0.68	0.8364	0.51997	Int-2.4	—
Hui	Pb-5.8Sb	40	10	209.9	27.3	0.0095	5.9	565.8	0.903	0.3532	0.08929	tendency	—
Hui	Pb-5.8Sb	40	30	205.1	27.3	0.0032	3.3	376.8	0.911	0.1571	0.01897	—	—
Wu	Pb-5.8Sb	40	5	219	27.3	0.0189	8.4	728.1	—	0.5834	0.24339	Int-1	—
Sb(6)	Pb-2.2Sb	140	10	149	95.6	0.0869	9.8	316.0	0.844	0.00415	0.00930	—	—
Sb(9)	Pb-2.2Sb	140	30	125	95.6	0.029	5.4	204.7	0.982	0.00181	0.0014	—	—
Hui	Pb-2.2Sb	40	3	258.4	27.3	0.0827	18.1	773	0.902	0.09067	0.1608	—	—
Hui	Pb-2.2Sb	40	10	235.4	27.3	0.0249	9.5	494.6	1.076	0.03803	0.02248	—	—
Hui	Pb-2.2Sb	40	30	189.3	27.3	0.0083	5.4	319.6	1.058	0.01607	0.00420	—	—
SN15	Pb-10Sn	110	20	116	75.1	0.0363	5.7	287.3	1.0	0.00049	0.02548	—	—
(Ojha)DS4	Pb-23Sn	52	5	160	35.5	0.0347	8.4	683.9	—	0.02699	1.2268	surface	—
(Ojha)DS5	Pb-23Sn	52	2	188	35.5	0.0867	13.8	943.3	—	0.1543	4.9542	Int-1	—
(Song, 18 mm)L5	Pb-41.9Sn	20	6	224	13.6	0.0048	5.2	1058.6	0.593	0.00969	7.35	Int-1	—
(Song, 18 mm)L6	Pb-32Sn	60	8	159	40.9	0.0140	5.3	568	0.62	0.011	0.892	Surf-9	—
Rajesh 33.4_4a	Pb-33.4Sn	75	8	166	51.2	0.0168	5.2	523.5	0.87	0.00975	0.75572	Surf-2	—
4b	Pb-38.7Sn	75	8	137	51.2	0.0097	4.3	558.9	0.84	0.00701	1.075	Surf-1	—
4c	Pb-34Sn	17	30	172	11.6	0.001	2.6	609.9	0.92	0.00068	0.6782	Surf-1	—
3g	Pb-27.1Sn	17	1	240	11.6	0.03	15.1	2014.6	0.516	0.2387	54.58	Int-2	—
1A	Pb-16.5Sn	101	4	172	68.9	0.225	15.5	532.8	0.85	0.01724	1.84	Surf-1	—
5a	Pb-57.9Sn	105	10	234	71.7	0.0066	3.0	498.0	0.93	0.00416	1.05971	—	—
5b	Pb-54.7Sn	67	40	177	45.7	0.0012	1.6	365.6	0.97	0.00040	0.25595	—	—
3c	Pb-23.4Sn	77	6	185	52.6	0.0421	7.6	553.8	0.86	0.02271	0.66169	Surf-2,3	—
3d	Pb-27Sn	59	64	155	40.3	0.0025	2.1	251.4	0.93	0.00023	0.03057	—	—
3f	Pb-30.3Sn	20	6	208	13.7	0.0072	6.4	975.4	0.712	0.01207	4.072	Int-2	—
3e	Pb-30Sn	8	0.35	194	5.5	0.0495	28.1	3842	—	1.47	625.4	Int-1	—
Sarazen thesis	Pb-10Sn	7.75	7.5	293	—	0.01	9.23	959.7	—	0.002115	0.976652	Int	7
10_In3	Pb-10Sn	1.43	18.3	383	—	0.0008	5.82	1372.1	—	0.000339	1.9717	Int	7
10_In5	Pb-10Sn	2.73	6.39	401	—	0.0042	9.99	1537.8	—	0.00235	3.8707	Int-3	7
10_In6	Pb-10Sn	3.47	23.3	368	—	0.0015	5.15	855.2	—	0.000248	0.4850	—	7
10_In7	Pb-10Sn	3.86	3.89	373	—	0.0096	12.19	1611.8	—	0.005317	5.28	Int	7
10_In10	Pb-10Sn	4.54	26.6	329	—	0.0017	4.81	726.64	—	0.000203	0.2924	—	7
10_In11	Pb-10Sn	5.18	3.06	374	—	0.0164	14.64	1573.7	—	0.009518	5.4897	Int	7
10_In12	Pb-10Sn	3.63	33.3	342	—	0.0011	4.29	732.8	—	0.000132	0.2802	—	7
10_In9	Pb-10Sn	4.64	16.6	355	—	0.0027	6.12	862.34	—	0.00047	0.5448	Int	7
H1_Laxmanan	Pb-14.9Sn	15.4	34.7	—	—	0.0017	3.2	448.17	1	0.000814	0.1114	—	8.9
H2	Pb-14.9Sn	16.8	12	—	—	0.0054	5.52	638.03	0.932	0.005083	0.4431	—	8.9
H3	Pb-15.30Sn	24.7	6.6	—	—	0.0139	7.42	681.98	0.775	0.01398	0.71044	—	8.9
H4	Pb-15.2Sn	22.3	4.1	—	—	0.0203	9.53	843.09	0.664	0.03077	1.5598	Int	8.9
H5	Pb-14Sn	34.3	2.1	—	—	0.0659	14.3	885.53	0.5	0.08525	2.60	Int	8.9
H6	Pb-15Sn	21.1	5.5	—	—	0.0145	8.23	773.72	—	0.019038	1.05	Int	8.9
Bergman	Pb-25Sn	4	125	—	—	0.0002	1.53	524.51	—	5×10^{-5}	0.2305	—	10
(35 × 63 mm)	Pb-25Sn	8	62.5	—	—	0.0006	2.19	490.58	—	0.000182	0.204	Surf-5,5	10
	Pb-25Sn	8	41.7	—	—	0.0009	2.7	569.5	—	0.000371	0.3572	Surf-4	10

Table I. (Continued) Growth Parameters and Rayleigh Numbers for Directionally Solidified Pb-Sb, Pb-Sn, and Al-Mg Alloys*

Sample	C_o (Wt Pct)	G_l (K cm^{-1})	V (μm s^{-1})	λ_{Expt} (μm)	G_{eff} (K cm^{-1})	S*	R_t (μm)	λ_{Theory} (μm)	k_e	R_{aB}	R_{aM}	Freckle	Reference
	Pb-25Sn	8	20.8	—	—	0.0018	3.84	735.7	—	0.001267	0.9326	Surf-2	10
	Pb-25Sn	4	20.8	—	—	0.0009	3.84	999.83	—	0.001162	2.15	Surf-1,2	10
	Pb-25Sn	8	10.4	—	—	0.0035	5.48	948.96	—	0.004319	2.39	Surf-1	10
	Pb-25Sn	4	10.4	—	—	0.0018	5.5	1282.4	—	0.00389	5.57	Surf-1	10
	Pb-25Sn	8	5.2	—	—	0.007	7.82	1222.4	—	0.0139	6.32	Int-1	10
Sarazin paper	Pb-5Sn	10.6	7.9	324	—	0.052	15.4	772.72	0.93	0.001475	0.1841	Int-5	6
	Pb-10Sn	10.3	8.09	295	—	0.012	8.9	837.54	0.85	0.001948	0.6507	Int-5	6
	Pb-20Sn	11.7	7.1	320	—	0.0093	7.45	898.35	0.86	0.01078	1.84	Int-4	6
	Pb-2Sb	9.25	9	390	—	0.0103	10.4	759.67	0.80	0.2225	0.06311	Int-7	6
	Pb-3Sb	10	8.3	350	—	0.0081	8.91	809.82	0.90	0.5286	0.1223	Int	6
Weinberg	Pb-20Sn	1.5	47	206?	1.0	0.0001	2.8	1339	—	0.00028	2.63	Int	5
Weinberg	Pb-20Sn	1.5	130	172?	1.0	0.0000	1.7	936	—	0.00004	1.17	Int	5
Weinberg	Pb-20Sn	2.3	110	119?	1.6	0.0000	1.8	802.7	—	0.00006	0.5573	—	5
Grugel *et al.*	Pb-45Sn	29	2	156	19.8	0.0193	9.16	1339	—	0.07236	24.78	Int	12
Mori *et al.*	Al-14Mg	27	7	—	16.3	0.0089	23.7	1888.3	—	0.01072	0.3401	Int	11
Mori *et al.*	Al-25Mg	26	9	—	15.7	0.0047	16.4	1891.4	—	0.00274	0.5974	Int	11

In this table, C_o is solute content of the alloy, G_l is the thermal gradient in the liquid at the dendrite tips, V is growth speed, λ_{Expt} is experimentally measured primary dendrite spacing, G_{eff} is the effective thermal gradient, S is the constitutional supercooling parameter, R_t is the dendrite tip radius and λ_{Theory} is the primary spacing predicted from the Hunt–Lu model,[18] R_{aB} is Rayleigh number following the procedure presented by Beckermann *et al.*,[16] and R_{aM} is the mushy-zone Rayleigh number, as defined in this article. The "Freckle" column lists the number of internal and surface freckles. The "Reference" column provides the appropriate references.

Fig. 4—Correlation between the severity of macrosegregation as given by the decrease in k_e *vs* the extent of mushy-zone convection as represented by an increasing Rayleigh number: (*a*) R_{aB} and (*b*) R_{aM}.

is true even when a set of data from one single investigator is examined. For example, in the Pb-5.8 and 2.2 wt pct Sb data set (SNT), channel segregates are absent at high R_{aB} of 1.06, but they are present at low R_{aB} of 0.25. The Pb-Sn alloy (SNT) and Pb-20 wt pct Sn (Weinberg) data also show similar behavior. Only the Pb-15 wt pct Sn (Wang), Pb-Sn alloys (Sarazin), and Pb-25 wt pct Sn (Bergman) data sets show distinct R_{aB} demarcations between segregate containing and segregate free samples. However, if we pool all of our samples together, then there is no correlation between R_{aB} and the formation of channels. Channel segregates are seen at the near minimum R_{aB} examined here, 4×10^{-5} for Pb-20 wt pct Sn (Weinberg data set), and also at the maximum R_{aB}, 0.9 for Pb-5.8 wt pct Sb (SNT data set), with channel-free and channel-containing samples scattered throughout the entire range of R_{aB}.

The mushy-zone Rayleigh number R_{aM}, which includes contribution of side branching in its permeability relationship, however, shows a significant improvement over R_{aB} in its ability to identify growth conditions that result in the formation of channel segregates; this is shown in Figure 5(b). Except for one experiment, marked as Pb-Sn alloys (Sarazin

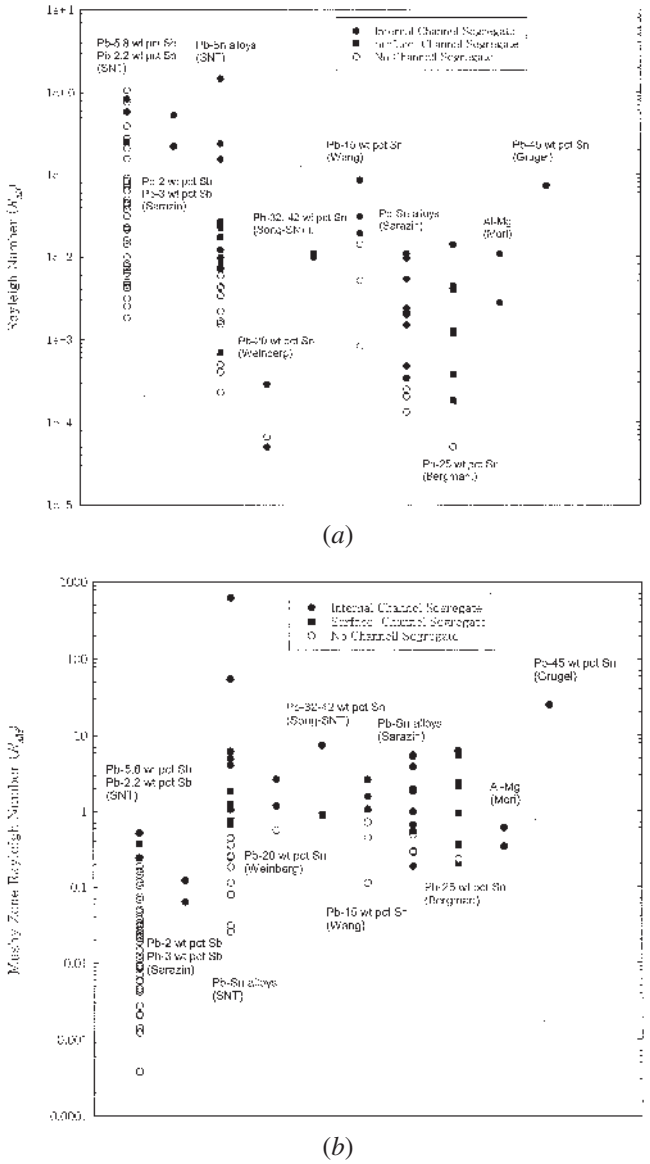

(*a*)

(*b*)

Fig. 5—Correlation between the channel segregate formation during directional solidification of metallic alloys and the extent of mushy-zone convection as represented by the Rayleigh number: (*a*) R_{aB} and (*b*) R_{aM}.

data set), all the data from within any single group now show distinct boundary between channel-free and channel-containing samples. Let us first examine R_{aM} data from steady-state directional solidification experiments where thermal gradients and growth speeds are individually controlled, and therefore, use of R_{aM} is more valid as compared with the end-quench DS data sets. The Pb-Sn alloys (SNT data set) show that surface channels form when R_{aM} exceeds about 0.5 and internal channels form when it exceeds about 2. The larger 1.8-cm-diameter Pb-Sn alloy samples, Song-SNT data in Figure 5(b), also show the same behavior as the smaller 0.7-cm-diameter ones. However, the critical Rayleigh number for channel formation in Pb-Sb alloys (Pb-5.8 wt pct Sb, Pb-2.2 wt pct Sb SNT data set) is about 0.2. The difference between Pb-Sb and Pb-Sn alloys may be attributed to uncertainties in the alloy physical properties used in calculating R_{aM}. Considering thermal gradient and growth speed uncertainties associated with several end-quench DS experiments included in this figure, R_{aM} appears to be a good parameter for describing channel segregate formation. If we ignore the two Pb-2 and 3 wt pct Sb (Sarazin) data in Figure 5(b), then channel segregate formation in all these experiments in a range of alloys appears to correspond to a narrow band of R_{aM}, between 0.2 to 0.8. This is a significant improvement over the predictive ability of other Rayleigh numbers described in the literature.[16,23] It is also interesting to note that R_{aM} is based upon theoretically predicted primary dendrite spacing; unlike other mushy-zone Rayleigh numbers used in the literature, one does not need prior experimental measurements of primary spacing to calculate R_{aM}.

V. CONCLUSIONS

The Mushy-zone Rayleigh number (R_{aM}) defined recently,[14] which incorporates a permeability relationship that accounts for dendrite side branching, is a good parameter to represent the intensity of interdendritic convection during directional solidification of alloys where increasing solute content decreases the melt density. It not only shows a very good correlation between increased convection and decreased primary spacing,[14] it also shows an excellent correlation between experimentally observed longitudinal macrosegregation and convection. The parameter, R_{aM}, can be used as a predictive tool to describe channel formation during directional solidification.

ACKNOWLEDGMENT

This research was supported by a grant from the Microgravity Materials Science Research Program at the NASA–Marshall Space Flight Center (Huntsville, AL).

REFERENCES

1. S.N. Tewari and R. Shah: *Metall. Trans. A*, 1991, vol. 23A, pp. 3383-92.
2. S.N. Ojha, G. Ding, Y. Lu, J. Reye, and S.N. Tewari: *Metall. Mater. Trans. A*, 1999, vol. 30A, pp. 2167-71.
3. T.M. Pollock and W.H. Murphy: *Metall. Mater. Trans. A*, 1996, vol. 27A, pp. 1081-94.
4. A.F. Giemei and B.H. Lear: *Metall. Trans*., 1970, vol. 1, pp. 2185-92.
5. N. Streat and F. Weinburg: *Metall. Trans*., 1972, vol. 3, pp. 3181-84.
6. J.R. Sarazin and A. Hellawell: *Metall. Trans. A*, 1988, vol. 12A, pp. 1861-71.
7. J.R. Sarazin: Ph.D. Thesis, Michigan Technological University, 1990, pp. 1-190 (Table 4 on p. 71).
8. L. Wang, V. Laxmanan, and J.F. Wallace: *Metall. Trans. A*, 1988, vol. 19A, pp. 2687-94.
9. V. Laxmanan, A. Studer, L. Wang, J.F. Wallace, and E.A. Winsa: NASA TM 89885, NASA, 1986, pp. 1-35.
10. M.I. Bergman, D.R. Fearn, J. Bloxham, and M.C. Shannon: *Metall. Mater. Trans. A*, 1997, vol. 28A, pp. 859-66.
11. N. Mori and O. Keisaku: *Metall. Trans. A*, 1991, vol. 22A, pp. 1663-72.
12. R.N. Grugel, A. Fedoseyev, and S. Kim: *Metall. Mater. Trans. A*, 2002, vol. 33A, pp. 3876-77.
13. S.N. Tewari and R. Shah: *Metall. Mater. Trans. A*, 1996, vol. 27A, pp. 1353-62.
14. S.N. Tewari and R. Tiwari: *Metall. Mater. Trans. A*, 2003, vol. 34A, pp. 2365-76.
15. *Transport Phenomena in Metallurgy*, G.H. Geiger and D.R. Poirier, eds., Addison-Wesley Publishing Company, New York, NY, 1973, p. 92.

16. C. Beckermann, J.P. Gu, and W.J. Boettinger: *Metall. Mater. Trans. A*, 2000, vol. 31A, pp. 2545-52.
17. P.K. Sung, D.R. Poirier, and S.D. Felicelli: *Metall. Mater. Trans. A*, 2001, vol. 22A, pp. 202-07.
18. J.D. Hunt and S.Z. Lu: *Metall. Mater. Trans. A*, 1996, vol. 27A, pp. 611-23.
19. M.D. Dupouy, D. Camel, and J.J. Favier: *J. Cryst. Growth*, 1993, vol. 126, pp. 480-88.
20. M.D. Dupouy, D. Camel, and J.J. Favier: *Acta Metall.*, 1989, vol. 37, pp. 1143-57.
21. R. Trivedi, H. Miyahara, P. Mazumder, E. Simsek, and S.N. Tewari: *J. Cryst. Growth*, 2000, vol. 222, pp. 365-79.
22. J.T. Mason, J.D. Verhoeven, and R. Trivedi: *J. Cryst. Growth*, 1982, vol. 59, pp. 516-24.
23. W. Yang, W. Chen, K.M. Chang, S. Mannan, and J. deBarbadillo: *Metall. Mater. Trans. A*, 2001, vol. 32A, pp. 397-403.